International Journal of
*Environmental Research and Public Health*

MDPI

*Article*

# The Drag Crisis Phenomenon on an Elite Road Cyclist—A Preliminary Numerical Simulations Analysis in the Aero Position at Different Speeds

**Pedro Forte [1,2,3,*], Jorge E. Morais [1,2,3], Henrique P. Neiva [3,4], Tiago M. Barbosa [2,3] and Daniel A. Marinho [3,4]**

[1] Department of Sports, Douro Higher Institute of Educational Sciences, 4560-708 Penafiel, Portugal; morais.jorgestrela@gmail.com
[2] Department of Sports Sciences and Physical Education, Instituto Politécnico de Bragança, 5300-253 Bragança, Portugal; barbosa@ipb.pt
[3] Research Center in Sports, Health and Human Development, CIDESD, 6201-001 Covilhã, Portugal; henriquepn@gmail.com (H.P.N.); marinho.d@gmail.com (D.A.M.)
[4] Department of Sports Science, Beira Interior University (UBI), 6201-001 Covilhã, Portugal
* Correspondence: pedromiguel.forte@iscedouro.pt; Tel.: +351-255-318-550

Received: 15 May 2020; Accepted: 9 July 2020; Published: 11 July 2020

**Abstract:** The drag crisis phenomenon is the drop of drag coefficient ($C_d$) with increasing Reynolds number (Re) or speed. The aim of this study was to assess the hypothetical drag crisis phenomenon in a sports setting, assessing it in a bicycle–cyclist system. A male elite-level cyclist was recruited for this research and his competition bicycle, helmet, suit, and shoes were used. A three-dimensional (3D) geometry was obtained with a 3D scan with the subject in a static aero position. A domain with 7 m of length, 2.5 m of width and 2.5 m of height was created around the cyclist. The domain was meshed with 42 million elements. Numerical simulations by computer fluid dynamics (CFD) fluent numerical code were conducted at speeds between 1 m/s and 22 m/s, with increments of 1 m/s. The drag coefficient ranged between 0.60 and 0.95 across different speeds and Re. The highest value was observed at 2 m/s ($C_d$ = 0.95) and Re of $3.21 \times 10^5$, whereas the lower $C_d$ was noted at 9 m/s ($C_d$ = 0.60) and $9.63 \times 10^5$. A drag crisis was noted between 3 m/s and 9 m/s. Pressure $C_d$ ranged from 0.35 to 0.52 and the lowest value was observed at 3m/s and the highest at 2 m/s. The viscous drag coefficient ranged between 0.15 and 0.43 and presented a trend decreasing from 4 m/s to 22 m/s. Coaches, cyclists, researchers, and support staff must consider that $C_d$ varies with speed and Re, and the bicycle–cyclist dimensions, shape, or form may affect drag and performance estimations. As a conclusion, this preliminary work noted a drag crisis between 3 m/s and 9 m/s in a cyclist in the aero position.

**Keywords:** cycling; drag coefficient; drag crisis; numerical simulations

## 1. Introduction

Athletes aim to save any time they are able to in time-based sports such as cycling. To improve their winning time, practitioners can employ a comprehensive set of techniques and methodologies [1,2]. Performance in time-based sports depends on speed [3]. In cycling, speed is the balance between mechanical power to overcome resistive forces and the mechanical power delivered [4]. In this sport it is possible to identify two main resistive forces: the drag and rolling resistance [4]. Rolling resistance is mainly dependent on the mass of the bicycle–cyclist system, speed, and rolling resistance

coefficient, whereas drag is dependent on speed, drag coefficient, fluid density, and surface area. The mean speed of professional road cyclists during a stage is about 40 km/h (≈ 11m/s) [5].

Drag accounts for 90% and rolling resistance for about 10% of the total resistive forces [6]. It is possible to assess resistive forces by experimental tests, analytical procedures and numerical simulations [2]. Numerical simulations by computational fluid dynamics (CFD) enable the assessment of aerodynamics in highly-controlled conditions. They show good adherence to experimental data from wind tunnel testing [2,7,8]. Moreover, CFD enables the breakdown of the total drag force into its components (pressure and viscous drag) [7–12].

The variable selected most often to assess aerodynamics is the effective surface area (product of frontal surface by drag coefficient, $C_d$) [4,8,9]. However, some analysts used to assume the drag coefficient ($C_d$) was invariant at different speeds [13,14]. Notwithstanding, variations in effective surface area have been explained by a phenomenon known as drag crisis. The drag crisis is a drop in $C_d$ at different Re and speeds due to a shift in the fluid flow behavior [9,15]. The fluid flow behavior around a body affects the $C_d$ [8,16]. A low flow speed, of about $Re = 2 \times 10^5$, is called a sub-critical regime [17]. A high Re value is known as a critical regime [18]. The super-critical regime is characterized by the transition from the laminar to turbulent flow. In a super-critical regime the Re is higher than in a critical regime [17–19]. The drag crisis has been reported in cycling [20] and spheres [15,21,22] and seems to occur at Re numbers between $4 \times 10^5$ and $8 \times 10^5$ [15]. The Re when that drag crisis occurs is called critical Re [15,20]. It was reported that for smooth spheres, the $C_d$ drops, reaching a bottom at the end of the critical regime (i.e., $3.5 \times 10^5 < Re < 5 \times 10^5$). Then, $C_d$ seems to rise at around $Re = 6.5 \times 10^5$ and $Re = 10^6$ [19]. The transition from a sub-critical to super-critical regime encompasses the transition from laminar to turbulent flow regime [15,20]. This transition is characterized by high pressure and flow velocity variations, whereas laminar flow is characterized by the non-disruption of fluid flow layers [15].

As far as the authors' understanding goes, only two papers have assessed the drag crisis in cycling, notably on a cyclist's leg [20] and the wake length influence on Re [23]. However, no study has reported the $C_d$ variations across different speeds on an elite road cyclist. Most studies assessing the drag crisis are conducted with smooth spheres, balls, and aerofoils [15,21,22]. No study was found with more complex geometries such as a bicycle–cyclist system. Little evidence on such a phenomenon is found in sports. Indeed, the drag crisis might occur in different bodies in sports settings just as in a bicycle–cyclist system. Forte et al. [24] suggested assessing $C_d$ across different speeds, even though, at least in sports sciences, analysts and researchers are prone to assume that $C_d$ is kept constant across a range of speeds [25].

It is a standard procedure to test cyclists in the aero position [24,25]. However, it is yet unclear if the phenomenon under appreciation is present when testing cyclists in the aero position. If so, it can explain, at least to some extent, drag variations as noted beforehand [24–26]. A deeper insight into the drag crisis and its effect on drag force can also be an aid to end-users. It can help end-users (cyclists, coaches, analysists, etc.) to run more accurate aerodynamics and performance forecasts.

The aim of this study was to assess the hypothetical drag crisis phenomenon in a sports setting, assessing it in a bicycle–cyclist system. It was hypothesized that a drag crisis phenomenon would be observed in a bicycle–cyclist system.

## 2. Materials and Methods

### *2.1. Subject*

A male elite level cyclist was recruited for this research. The subject participated in national competitions, weighed 65.00 kg and was 1.76 m tall; the bicycle weighed 7 kg. The subject's height was measured with the participant looking forward, shoulders relaxed, arms at sides, legs straight and knees together, the feet flat and heels almost together. The participant had an upper leg length of 0.60 m, shoulder/biacromial breadth of 0.39 m, biiliac breadth of 0.32 m, upper arm length of 0.36 m, abdominal circumference of 0.76 m, arm circumference 0.32 m, hip circumference 0.98 m, and thigh circumference 0.54 m. The skin folds were not measured. All procedures were in accordance

with the Helsinki Declaration regarding human research and informed written consent by the volunteer subject was obtained beforehand. The scientific committee of the Higher Institute of Educational Sciences of the Douro approved the research (PROJ1.576).

### *2.2. Scanning the Model*

The subject and bicycle were scanned in the aero position (Figure 1). The cyclist wore racing clothes, shoes and helmet, and used his own bicycle. The subject was asked to maintain a static position during scanning. The bicycle was placed and fixed on a roller.

**Figure 1.** The meshed geometry in the aero position.

The scans were collected by a portable Sense 3D scanner (3D Systems, Inc., Rock Hill, SC, USA) and saved in the Sense Software (Sense, 3D Systems, Inc., Rock Hill, SC, USA). The scanner precision was 0.0009 m (0.9 mm) at 0.5 m (50 cm) distance. The Sense software allowed us to clean, fill holes and solidify the entire bicycle–cyclist geometry, then the model was exported as a stereolithographic file (.stl) [27]. The CAD models were created in Geomagic studio software (3D Systems, Rock Hill, SC, USA) [9].

### *2.3. Boundary Conditions*

The Ansys Workbench geometry module software (Ansys Fluent 16.0, Ansys Inc., Canonsburg, PA, USA) enabled us to create a three-dimensional domain (length = 7 m; width = 2.5 m; height = 2.5 m) around the cyclist. The domain was meshed with more than 42 million elements to represent the fluid. The elements were prismatic and tetrahedral with cell size near 25.72 μm. The cyclist geometry was at 2.5 m from the inlet portion for each simulation [28].

Typically, a professional road cyclist reaches mean speeds of about 11 m/s (≈ 40 km/h) during a stage [5]. Thus, the numerical simulations were conducted between 1 and 22 m/s with increments of 1 m/s (22 speeds). The speeds were set at the inlet portion of the enclosure (-z direction). The

turbulence intensity was assumed as $1 \times 10^{-6}$% for different positions. The non-slip wall and scalable wall functions were assigned.

### *2.4. Numerical Simulations*

The Reynolds-averaged Navier–Stokes (RANS) equations in fluent CFD code are solved by the finite volumes approach method. To solve these equations a turbulence model is required; the realizable k-ε was selected and the SIMPLE algorithm was used to solve the correction in velocities and pressure and satisfy the discrete continuity equation of the fluid flow behavior. The governing equations of the discretization schemes were defined as second order and the gradients were computed by the least-squares cell-based method. Pressure and momentum were set as second order and second order upwind. The turbulent kinetic energy and dissipation rate were defined as first order upwind [12]. The convergence occurred automatically in the Ansys Fluent 16.0 [24–27].

### *2.5. Outcomes*

#### 2.5.1. Drag Force

The numerical simulations allows us to obtain the drag and the drag coefficient from Ansys Fluent Software [24–27]. For the drag force, Equation (1) was used:

$$F_d = \frac{1}{2}\rho A C d v^2 \quad (1)$$

where $F_d$ is the drag force, $C_d$ represents the drag coefficient, v the velocity, A the surface area and ϱ is the air density (1.292 kg/m$^3$) [24–27]. $C_d$ is given by Equation (2):

$$C_d = \frac{\frac{1}{2}pAv^2}{F_d} \quad (2)$$

#### 2.5.2. Reynolds Number

Reynolds number was calculated as:

$$R_e = \frac{pvL}{\mu} \quad (3)$$

where L is the characteristic linear dimension and μ is the dynamic viscosity of the fluid (assumed as 0.00001813 Pa/s).

## 3. Results

Drag coefficient variations are presented across different speeds and Re in Figure 2 (top panel). The highest value was observed at 2 m/s ($C_d$ = 0.95) with a Re of $3.21 \times 10^5$. The lower $C_d$ was noted at 9 m/s ($C_d$ = 0.60) and $9.63 \times 10^5$. The partial difference between lowest and highest $C_d$ was 37%. The $C_d$ seems to increase from 1 to 2 m/s (Re of $1.07 \times 10^5$ to $2.14 \times 10^5$) and drops to 3m/s (Re = $3.21 \times 10^5$). It is then possible to identify another $C_d$ decay between 4 m/s (Re = $4.28 \times 10^5$) and 9 m/s (Re = $9.63 \times 10^5$). Afterwards, $C_d$ increases from 9 m/s (Re = $9.63 \times 10^5$) to 10 m/s (Re = $1.07 \times 10^6$) and decreased from 10 m/s (Re = $1.07 \times 10^6$) to 22 m/s (Re = $2.35 \times 10^6$). Thus, a drag crisis between 3m/s and 9m/s in the bicycle–cyclist system was noted.

Pressure $C_d$ ranged from 0.35 to 0.52 and (Figure 2, middle panel). The partial change between lowest and highest values was 33% (Figure 2, middle panel). The lowest value was observed at 3m/s and the highest at 2 m/s. Pressure $C_d$ seemed to increase from 1 m/s to 2 m/s and then decreased at 3 m/s. Pressure $C_d$ had variations up to 7%, between 3 and 9 m/s. From 9 m/s to 22 m/s, the pressure $C_d$ increased from 19% to 21%. Altogether, a crisis phenomenon was also noted in the pressure $C_d$ between 3m/s and 9m/s.

Viscous $C_d$ values ranged between 0.15 and 0.43, and the partial variation was 65% (Figure 2 bottom panel). A trend for viscous $C_d$ to increase from 1 m/s to 2 m/s and then decrease to 3 m/s was

observed. From 4 m/s onwards, viscous $C_d$ decreased between 5% and 44%. Therefore, the drag crisis did not seem to be as obvious as in pressure $C_d$ and it can be argued that it had less influence on the total $C_d$ drop.

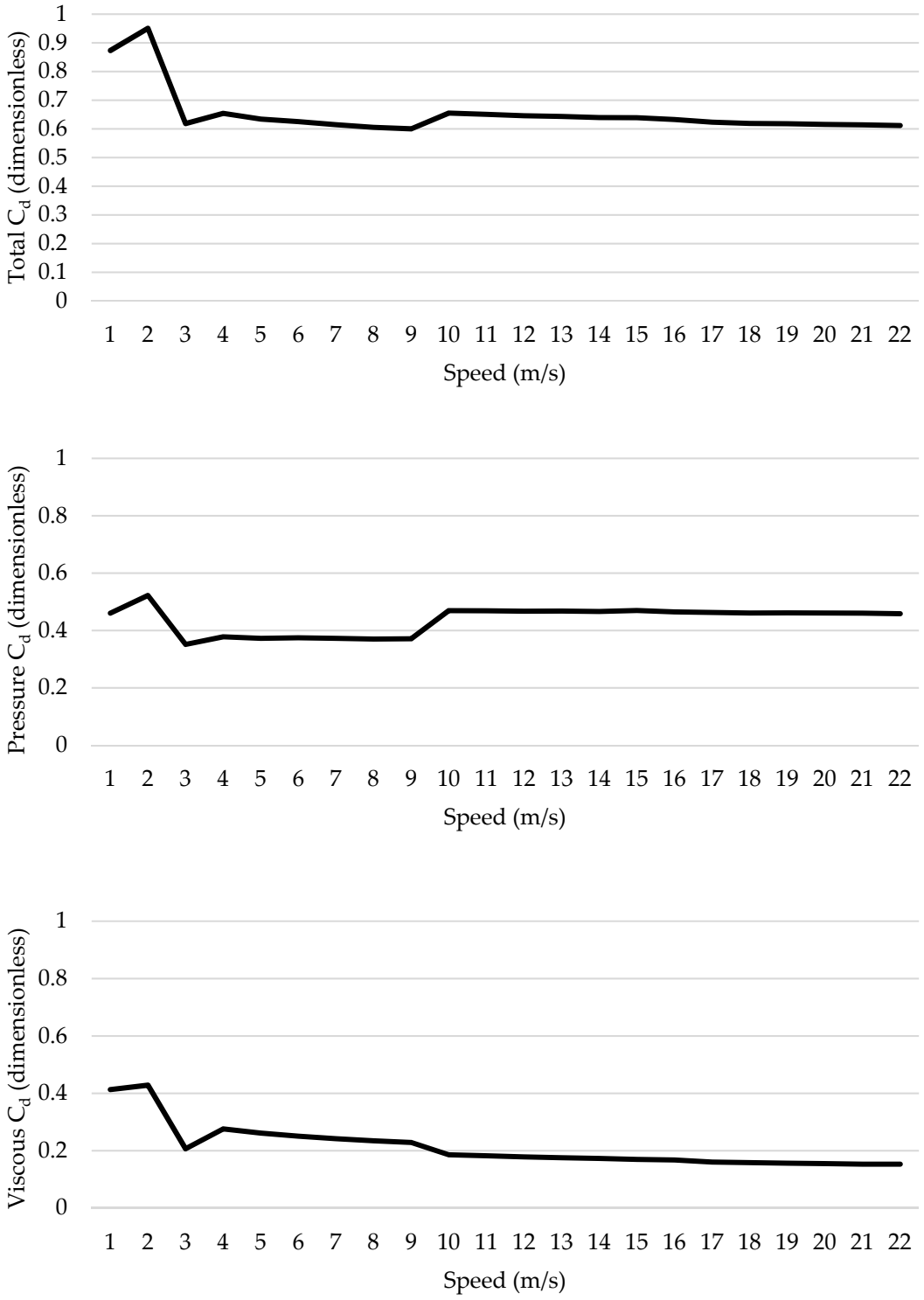


**Figure 2.** Drag coefficient ($C_d$) variations across different speeds (top panel), pressure drag coefficient (middle panel) and viscous drag coefficient (bottom panel) across different speeds.

## 4. Discussion

The aim of this study was to assess the hypothetical drag crisis phenomenon in a sports setting, assessing it in a bicycle–cyclist system. It was verified that total, pressure and viscous $C_d$ differed across the different speeds. A $C_d$ drop was noted from 3 m/s to 9 m/s and from Re = $3.21 \times 10^5$ to $9.63 \times 10^5$.

In the current study, $C_d$ ranged between 0.60 and 0.95, from 1 m/s to 22 m/s, and it varied between 0.3% and 35%. From 1 m/s to 3 m/s, the $C_d$ increased and decreased over the selected speed range. A decreasing trend was observed from 3 m/s to 9 m/s, and between 10 m/s and 22 m/s the $C_d$ presented a trend to decrease with speed. Altogether, the drag crisis was observed between 3 m/s and 9 m/s and $C_d$ stabilized for speeds above 10 m/s. The $C_d$ depends on the fluid flowing around the body [8,16] and the fluid flow is dependent on the body's geometry or shape [8,16]. Moreover, the drop in $C_d$ values can be explained by the fluid flow transition from laminar to turbulent. The fluid flow is characterized as sub-critical in laminar flows [15,20]. In this regime, the $C_d$ seems not to be stable, and may explain the variations between 1 m/s and 3 m/s due to the fluid layers' viscosity breakup [15]. The dragged fluid on the body surface disrupts due to the speed and turbulence and, after the critical regime, it is expected that $C_d$ reaches the bottom value [19]. The critical regime seems to end at Re between $3.5 \times 10^5$ and $5 \times 10^5$ [19]. However, in the current study, the lowest $C_d$ = 0.60 was achieved at Re = $9.63 \times 10^5$. The fluid flow transitions have been evaluated in spheres or airfoils [15,21,22]. An analysis with soccer ball aerodynamics revealed that drag crisis occurs near 8 m/s to 18 m/s and $C_d$ drops from 0.5 to 0.15 [29]. Yand and Cheng [30] performed a hydrodynamic analysis of a cylinder drag crisis with an O-tube and revealed that $C_d$ reduced from 0.9 to 0.35 at Re between $1.9 \times 10^5$ and $2.7 \times 10^5$. Conversely, in more complex geometries such as a bicycle–cyclist system, it was yet unclear if the same phenomenon would be present. For a cyclist in the time trial position, a position similar to the aero position, the $C_d$ is 0.60 at Re = $7 \times 10^5$ [31,32]. In this study, $C_d$ was near 0.60 at $7.49 \times 10^5 < \text{Re} < 9.63 \times 10^5$.

The total $C_d$ is given by the sum of pressure and viscous $C_d$. Pressure $C_d$ varied from 0.35 and 0.52, and viscous $C_d$ between 0.15 and 0.43. The pressure $C_d$ partial contribution to total $C_d$ was between 53% and 75%; whereas, viscous $C_d$ was between 25% to 47%. The partial contribution of pressure $C_d$ increased with speed and, conversely, viscous $C_d$ contribution decreased with speed. This seems to be in agreement with the literature. Authors have reported that pressure drag is the main force responsible for aerodynamic resistance [26,28,31–33]. In the current study, the drag crisis phenomenon was noticeable in pressure $C_d$ between 3 m/s and 9 m/s and Re $3.21 \times 10^5$ and $9.63 \times 10^5$. This phenomenon seems to be related to the flow regimes transition (critical regime) from laminar to turbulent flow [15,19]. In the present study, it seems that the flow transitions happened between 3 m/s and 9 m/s. The viscous $C_d$ mainly decreased with speed. Therefore, based on these findings it seems that viscous $C_d$ is not responsible for the drag crisis phenomenon. Viscous drag encompasses the interaction between the body's surface and the fluid [15]. Thus, due to the fluid flow transitions, viscous drag had a small contribution in comparison to pressure drag, as speed increases [9,15]. In the current research, the fluid (air) was dragged by sublayers to the bicycle–cyclist system surface. The dragged fluid on the body forms the first layer and the following layer of fluid is dragged to the previous layer [15]. As speed increases, viscous $C_d$ seems to decrease, and the dragged fluid on the surface disrupts the body due to the flow turbulence. Thus, the fluid flow turbulence is the one responsible for disrupting the dragged flow sublayers to the object and, as less fluid is dragged to the cyclist, there is less viscous drag [15]. Upon that, pressure drag was the main force responsible for the drag crisis.

This was the first attempt to assess the drag crisis phenomenon on a bicycle–cyclist system. Altogether, the drag crisis phenomenon seems to occur at speeds between 3 m/s and 9 m/s and Re is from $3.21 \times 10^5$ to $9.63 \times 10^5$ in the recruited bicycle–cyclist system. This phenomenon was firstly reported with spheres, and at different ranges of Re than what is reported in the present study. With no surprise, the different ranges of Re where drag crisis is noted should be related to differences in the bodies´ geometries. Out of the two drag components, pressure $C_d$ is the one explaining the drag crisis; conversely, the role of viscous $C_d$ is minimal. Several studies forecasting the cyclist´s

aerodynamics and performance assume $C_d$ as invariant across different speeds [24–27]. Taking into consideration the drag crisis and how it affects the $C_d$, it might increase the accuracy of such forecasts in the future. Therefore, end-users, including coaches, cyclists, researchers and support staff should be aware of these $C_d$ variations when running forecasts and models. Altogether, both viscous and pressure drag coefficients contribute to the drag crisis. At lower speeds (<5 m/s), the viscous drag coefficient has higher variation in comparison to the pressure drag coefficient. This might be due to the fluid flow behavior and the disruption of the fluid from the body surface (viscous drag) due to turbulence [15].

The limitations of this research are: (i) The simulations were run in just one position and $C_d$ varies in different positions. Thus, the range of speeds and Re at which the drag crisis happens might vary across different positions. (ii) One single elite cyclist was recruited. As such, care should be exercised extrapolating these results to other demographics (e.g., age groups or para-cycling) and competitive levels. In future work it is important to assess the drag crisis phenomenon on different cycling positions. Moreover, a para-cyclist may have different forms/shapes due to the prosthesis used. Upon that, it is important to assess this phenomenon in different geometries and present the $C_d$ variations, wake flow behavior with streamlines, and vorticity at the selected speeds. Moreover, with the intention to simulate different subjects, simulations with higher or lower surface areas might be performed with the same bicycle–cyclist model.

## 5. Conclusions

The $C_d$ variations of a bicycle–cyclist system differ from different object forms. This may suggest that the cyclists' different adopted positions might have different $C_d$ variations and the drag crisis phenomenon may vary between positions and body forms. In conclusion, a drag crisis phenomenon is noted in a bicycle–cyclist system in the aero position. The crisis happens at speeds from 3 m/s to 9 m/s and Re between $3.21 \times 10^5$ and $9.63 \times 10^5$. The drag crisis is mostly due to a crisis in pressure $C_d$. It is important to consider extrapolating the results to different competitive levels or cyclists due to different body sizes and measurements.

**Author Contributions:** Conceptualization, P.F., H.P.N., J.E.M.; methodology, D.A.M. and T.M.B.; software, P.F., J.E.M. and D.A.M.; validation, T.M.B. and J.E.M.; formal analysis, P.F., H.P.N. and J.E.M.; investigation, P.F., H.P.N. and J.E.M.; resources, D.A.M.; data curation, P.F. and J.E.M.; writing—original draft preparation, P.F. and H.P.N.; writing—review and editing, T.M.B. and J.E.M.; supervision, D.A.M. and T.M.B.; funding acquisition, D.A.M. All authors have read and agreed to the published version of the manuscript.

**Funding:** This research is supported by the Portuguese Foundation for Science and Technology, I.P. (project UIDB04045/2020) and The APC was funded by Research Center in Sports Health and Human Development, Covilhã, Portugal.

**Conflicts of Interest:** The authors declare no conflict of interest.

## References

1. Barbosa, T.M.; Morais, J.E.; Forte, P.; Neiva, H.P.; Garrido, N.D.; Marinho, D.A. Correction: A Comparison of Experimental and Analytical Procedures to Measure Passive Drag in Human Swimming. *PLoS ONE* **2017**, *12*, e0177038, doi:10.1371/journal.pone.0177038.
2. Forte, P.; Barbosa, T.M.; Marinho, D.A. *Technologic Appliance and Performance Concerns in Wheelchair Racing—Helping Paralympic Athletes to Excel. New Perspectives in Fluid Dynamics*; Chaoqun, L., Ed.; IntechOpen: Rijeka, Croatia, 2015; pp. 101–121.
3. Paton, C.; Hopkins, W.G. Variation in performance of elite cyclists from race to race. *Eur. J. Sport Sci.* **2006**, *6*, 25–31, doi:10.1080/17461390500422796.
4. Martin, J.C.; Milliken, D.L.; Cobb, J.E.; McFadden, K.L.; Coggan, A.R. Validation of a Mathematical Model for Road Cycling Power. *J. Appl. Biomech.* **1998**, *14*, 276–291, doi:10.1123/jab.14.3.276.
5. El Helou, N.; Berthelot, G.; Thibault, V.; Tafflet, M.; Nassif, H.; Campion, F.; Hermine, O.; Toussaint, J.-F. Tour de France, Giro, Vuelta, and classic European races show a unique progression of road cycling speed in the last 20 years. *J. Sports Sci.* **2010**, *28*, 789–796, doi:10.1080/02640411003739654.

6. Candau, R.B.; Grappe, F.; Mernard, M.; Barbier, B.; Millet, G.Y.; Hoffman, M.D.; Belli, A.R.; Rouillon, J.D. Simplified deceleration method for assessment of resistive forces in cycling. *Med. Sci. Sports Exerc.* **1999**, *31*, 1441–1447, doi:10.1097/00005768-199910000-00013.
7. Defraeye, T.; Blocken, B.; Koninckx, E.; Hespel, P.; Carmeliet, J. Aerodynamic study of different cyclist positions: CFD analysis and full-scale wind-tunnel tests. *J. Biomech.* **2010**, *43*, 1262–1268, doi:10.1016/j.jbiomech.2010.01.025.
8. Debraux, P.; Grappe, F.; Manolova, A.V.; Bertucci, W. Aerodynamic drag in cycling: Methods of assessment. *Sports Biomech.* **2011**, *10*, 197–218, doi:10.1080/14763141.2011.592209.
9. Forte, P.; Marinho, D.A.; Morais, J.E.; Morouço, P.G.; Barbosa, T.M. The variations on the aerodynamics of a world-ranked wheelchair sprinter in the key-moments of the stroke cycle: A numerical simulation analysis. *PLoS ONE* **2018**, *13*, e0193658, doi:10.1371/journal.pone.0193658.
10. Forte, P.; Marinho, D.; Morais, J.E.; Morouço, P.; Barbosa, T.M. Estimation of mechanical power and energy cost in elite wheelchair racing by analytical procedures and numerical simulations. *Comput. Methods Biomech. Biomed. Eng.* **2018**, *21*, 585–592, doi:10.1080/10255842.2018.1502277.
11. Beaumont, F.; Taiar, R.; Polidori, G.; Trenchard, H.; Grappe, F. Aerodynamic study of time-trial helmets in cycling racing using CFD analysis. *J. Biomech.* **2018**, *67*, 1–8, doi:10.1016/j.jbiomech.2017.10.042.
12. Defraeye, T.; Blocken, B.; Koninckx, E.; Hespel, P.; Carmeliet, J. Computational fluid dynamics analysis of cyclist aerodynamics: Performance of different turbulence-modelling and boundary-layer modelling approaches. *J. Biomech.* **2010**, *43*, 2281–2287, doi:10.1016/j.jbiomech.2010.04.038.
13. Olds, T.S.; Norton, K.I.; Lowe, E.L.; Olivé, S.; Reay, F.; Ly, S. Modeling road-cycling performance. *J. Appl. Physiol.* **1995**, *78*, 1596–1611, doi:10.1152/jappl.1995.78.4.1596.
14. Fintelman, D.; Sterling, M.; Hemida, H.; Li, F.X. Optimal cycling time trial position models: Aerodynamics versus power output and metabolic energy. *J. Biomech.* **2014**, *47*, 1894–1898, doi:10.1016/j.jbiomech.2014.02.029.
15. Schlichting, H. *Boundary Layer Theory*; McGraw-Hill: New York, NY, USA, 1979.
16. Pugh, L.G.C.E. The influence of wind resistance in running and walking and the mechanical efficiency of work against horizontal or vertical forces. *J. Physiol.* **1971**, *213*, 255–276, doi:10.1113/jphysiol.1971.sp009381.
17. Williamson, C.H. Vortex dynamics in the cylinder wake. *Annu. Rev. Fluid Mech.* **1996**, *28*, 477–539.
18. Perrin, R.; Braza, M.; Cid, E.; Cazin, S.; Moradei, F.; Barthet, A.; Sevrain, A.; Hoarau, Y. Near-Wake Turbulence Properties in the High Reynolds Number Incompressible Flow Around a Circular Cylinder Measured by Two- and Three-Component PIV. *Flow, Turbul. Combust.* **2006**, *77*, 185–204, doi:10.1007/s10494-006-9043-5.
19. Rodriguez, I.; Lehmkuhl, O.; Chiva, J.; Borrell, R.; Oliva, A. On the flow past a circular cylinder from critical to super-critical Reynolds numbers: Wake topology and vortex shedding. *Int. J. Heat Fluid Flow* **2015**, *55*, 91–103, doi:10.1016/j.ijheatfluidflow.2015.05.009.
20. Scarano, F.; Terra, W.; Sciacchitano, A. Investigation of the drag crisis on the leg of a cycling mannequin by means of robotic volumetric PIV. In Proceedings of the 15th International Conference on Fluid Control, Measurements and Visualization, Napoles, Italy, **2019**; pp.1–9.
21. Vakarelski, I.U.; Chan, D.Y.C.; Thoroddsen, S.T. Leidenfrost vapour layer moderation of the drag crisis and trajectories of superhydrophobic and hydrophilic spheres falling in water. *Soft Matter* **2014**, *10*, 5662–5668, doi:10.1039/c4sm00368c.
22. Geier, M.; Pasquali, A.; Schönherr, M. Parametrization of the cumulant lattice Boltzmann method for fourth order accurate diffusion part II: Application to flow around a sphere at drag crisis. *J. Comput. Phys.* **2017**, *348*, 889–898, doi:10.1016/j.jcp.2017.07.004.
23. Terra, W.; Sciacchitano, A.; Scarano, F. Cyclist Reynolds number effects and drag crisis distribution. *J. Wind. Eng. Ind. Aerodyn.* **2020**, *200*, 104143, doi:10.1016/j.jweia.2020.104143.
24. Forte, P.; Marinho, D.A.; Nikolaidis, P.T.; Knechtle, B.; Barbosa, T.M.; Costa, M.J. Analysis of Cyclist's Drag on the Aero Position Using Numerical Simulations and Analytical Procedures: A Case Study. *Int. J. Environ. Res. Public Heal.* **2020**, *17*, 3430, doi:10.3390/ijerph17103430.
25. Forte, P.; Marinho, D.A.; Barbosa, T.M.; Morouço, P.; Morais, J.E. Estimation of an Elite Road Cyclist Performance in Different Positions Based on Numerical Simulations and Analytical Procedures. *Front. Bioeng. Biotechnol.* **2020**, *8*, 538, doi:10.3389/fbioe.2020.00538.

26. Forte, P.; Marinho, D.A.; Silveira, R.; Barbosa, T.M.; Costa, M.J. The Aerodynamics and Energy Cost Assessment of an Able-Bodied Cyclist and Amputated Models by Computer Fluid Dynamics. *Medicina* **2020**, *56*, 241, doi:10.3390/medicina56050241.
27. Forte, P.; Marinho, D.A.; Barbosa, T.M.; Morais, J.E. Analysis of a normal and aero helmet on an elite cyclist in the dropped position. *AIMS Biophys.* **2020**, *7*, 54–64, doi:10.3934/biophy.2020005.
28. Blocken, B.; Defraeye, T.; Koninckx, E.; Carmeliet, J.; Hespel, P. CFD simulations of the aerodynamic drag of two drafting cyclists. *Comput. Fluids* **2013**, *71*, 435–445, doi:10.1016/j.compfluid.2012.11.012.
29. Goff, J.E.; Kelley, J.; Hobson, C.M.; Seo, K.; Asai, T.; Choppin, S.B. Creating drag and lift curves from soccer trajectories. *Eur. J. Phys.* **2017**, *38*, 044003, doi:10.1088/1361-6404/aa6fcd.
30. Yang, F.; An, H.; Cheng, L. Drag crisis of a circular cylinder near a plane boundary. *Ocean Eng.* **2018**, *154*, 133–142, doi:10.1016/j.oceaneng.2018.01.011.
31. Crouch, T.; Burton, D.; Labry, Z.A.; Blair, K.B. Riding against the wind: A review of competition cycling aerodynamics. *Sports Eng.* **2017**, *20*, 81–110, doi:10.1007/s12283-017-0234-1.
32. Blocken, B.; Van Druenen, T.; Toparlar, Y.; Andrianne, T. Aerodynamic analysis of different cyclist hill descent positions. *J. Wind. Eng. Ind. Aerodyn.* **2018**, *181*, 27–45, doi:10.1016/j.jweia.2018.08.010.
33. Gibertini, G.; Grassi, D. *Cycling Aerodynamics*; Nørstrud, H., Ed.; Springer: Vienna, Austria, 2008; pp. 23–47.